

# Photoactivation at a clinical LINAC: The $^{197}\text{Au}(\gamma,n)^{196}\text{Au}$ reaction slightly above threshold

P. Mohr<sup>a</sup> S. Brieger<sup>a</sup> G. Witucki<sup>a</sup> M. Maetz<sup>b</sup>

<sup>a</sup>*Strahlentherapie, Diakonie-Klinikum Schwäbisch Hall, Diakoniestraße 10, D-74523 Schwäbisch Hall, Germany*

<sup>b</sup>*Gymnasium bei St. Michael, Tüngentaler Str. 92, D-74523 Schwäbisch Hall, Germany*

---

## Abstract

The properties of a clinical LINAC are investigated for a study of photoactivation cross sections slightly above the neutron threshold. As an example, the photoactivation of a tiny amount of gold by the  $^{197}\text{Au}(\gamma,n)^{196}\text{Au}$  reaction has been measured. The derived photon intensity is at least comparable to conventional and widely used photon sources. In combination with its extremely stable operation, a clinical LINAC ensures that photoactivation studies can be performed for a wide number of targets with very limited beamtime.

*Key words:* bremsstrahlung, photoactivation, medical accelerators

*PACS:* 25.20.-x, 29.17.+w

---

## 1 Introduction

The technique of photoactivation has found applications in various fields [1,2]. At low-energy accelerators photoactivation experiments are restricted to isomers (see e.g. [3,4]); only few experiments have been carried out. The majority of photoactivation experiments is performed using bremsstrahlung with endpoint energies of about 20 – 30 MeV; in this case the huge cross section of the  $(\gamma,n)$  reaction around the giant dipole resonance at energies of about 15 MeV leads to excellent sensitivity of the photoactivation technique [2]. It

---

*Email address:* Peter.Mohr@diaksha.de (P. Mohr).

has been shown that medical accelerators are able to provide a sufficient photon intensity for such experiments [5]. In the present investigation we focus on photoactivation experiments at energies slightly above the neutron threshold which are feasible at a clinical linear accelerator (cLINAC) with relatively low photon energies up to 10 MeV.

The experimental study of photon-induced cross sections has found increasing interest in the last years. Most of the recent studies were motivated by the astrophysical relevance of photon-induced reactions in the so-called astrophysical  $p$ -process or  $\gamma$ -process where neutron-deficient heavy nuclei are synthesized by a series of  $(\gamma,n)$ ,  $(\gamma,\alpha)$ , and  $(\gamma,p)$  reactions at temperatures of about two to three billions Kelvin ( $T_9 = 2 - 3$ ) [6,7,8,9,10,11]. At such high temperatures the high-energy tail of the blackbody radiation spectrum has a sufficient intensity to induce a noticeable reaction rate for photon-induced reactions.

It has been shown that the astrophysically relevant energy window for  $(\gamma,n)$  reactions is located slightly above the threshold of the  $(\gamma,n)$  reaction and has a width of less than 1 MeV [12]; the position of this window is almost independent of the temperature  $T$ . In contrast the energy window for  $(\gamma,\alpha)$  reactions depends sensitively on the temperature  $T$  and has a much broader width of several MeV. The position and width can be estimated from the Gamow window of the inverse  $(\alpha,\gamma)$  capture reaction. The position is shifted by the  $Q$ -value of the  $(\alpha,\gamma)$  reaction ( $E_{(\gamma,\alpha)}^{\text{eff}} = E_{(\alpha,\gamma)}^{\text{eff}} + Q_\alpha$ ), and the width is practically identical as in the  $(\alpha,\gamma)$  reaction [13].

Recent experiments have been performed with almost monochromatic photons from laser Compton scattering (LCS) [11,14,15,16,17] as well as with continuous photon energy distributions from bremsstrahlung [11,12,18,19,20,21]. In addition, a new photon source using a superconducting wiggler at an electron storage ring with the energy of several GeV has been suggested [22,13].

It is the aim of the present work to compare the performance of previously used bremsstrahlung photon sources (e.g., S-DALINAC at TU Darmstadt or ELBE at Forschungszentrum Dresden in Rossendorf or commercially available electron accelerators) with the output of a cLINAC. In the present investigation we use the cLINAC of Diakoniekrankenhaus Schwäbisch Hall which is a standard cLINAC manufactured by Elekta, Crawley, United Kingdom. The measured yield from photoactivation of a gold sample via the  $^{197}\text{Au}(\gamma,n)^{196}\text{Au}$  reaction allows the determination of the number of photons in the clinically used photon beam because the cross section of this reaction has been studied carefully in a wide energy range [18,14,23]. We derive the number of photons at an energy of 9 MeV using a simplistic linear spectral distribution and a realistic photon spectrum from a GEANT simulation.

The paper is organized as follows. In Sect. 2 the general properties of the cLINAC are summarized. In Sect. 3 the experimental set-up for the photoactivation of gold by the  $^{197}\text{Au}(\gamma, n)^{196}\text{Au}$  reaction is presented. In Sect. 4 the experimental data are analyzed, and the photon density is derived from the measured photoactivation yield. The experimental results are discussed in Sect. 5 and compared to other photon sources in Sect. 6. Finally, conclusions are given in Sect. 7.

## 2 Properties of a clinical LINAC

The cLINAC under study is an up-to-date cLINAC which has been installed in 2005 by the manufacturer Elekta. The following schematic view of the cLINAC is summarized from the technical documentation of the cLINAC [24]. The very stable and reliable operation of a cLINAC under clinical conditions is an excellent basis for basic physics research. Typically a cLINAC is running every working day. The required maintenance is 7 days per year of operation. The manufacturer guarantees a 96 % availability which corresponds to 10 further days of unplanned maintenance per year. The overall availability of a cLINAC is more than 90 %. Such a high availability has indeed been achieved for the cLINAC under investigation in its first two years of operation including all its peripheral devices. The availability of the beam from the cLINAC is even better.

The primary electron beam is generated in a gun with an energy of about 50 keV leading to an injection velocity of about 40 % of the speed of light:  $v \approx 0.4 c$ . The electrons are accelerated in a copper cavity by 3 GHz radiofrequency (RF) with a peak power of about 5 MW in the pulse and with a pulse repetition frequency (PRF) of 200 Hz or 400 Hz (depending on the chosen energy). For an electron energy of 10 MeV a primary electron current of about 500 mA in the pulse can be roughly estimated assuming that 100 % of the RF power are converted into electron energy. Together with the PRF of 200 Hz and a typical pulse width of about  $3 \mu\text{s}$  this results in an average electron current of about  $300 \mu\text{A}$ .

Steering and focusing of the electron beam is achieved by standard magnetic and electrostatic devices. An achromatic bending system is used to transport the beam onto a massive tungsten target where the electron beam is stopped and bremsstrahlung with an endpoint energy identical to the primary kinetic electron energy is produced.

After a massive primary collimator with a thickness of about 10 cm the photon beam hits a flattening filter. The bremsstrahlung emission process is focused at forward angles. The shape of the flattening filter is optimized to obtain an

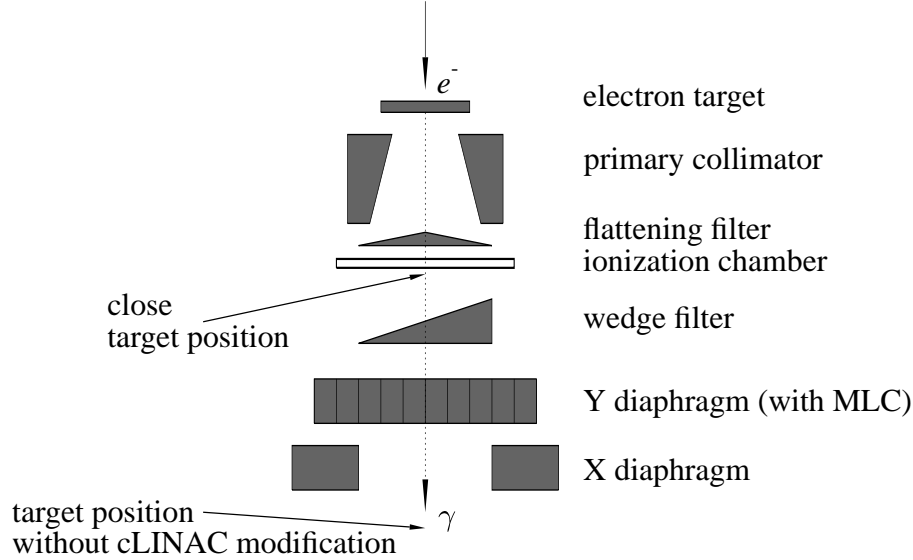


Fig. 1. Schematic view of the photon beam production and collimation of a cLINAC. Two target positions for photoactivation are shown: a close position at SSD  $\approx 20$  cm which requires some modification of the cLINAC and a second position at SSD  $\approx 55$  cm which can be used in the clinical set-up (see text).

almost flat photon angular distribution which finally has to deliver a flat dose profile to the patient. The distance from the almost point-like photon source to an irradiation position is called source-surface distance (SSD). A schematic view of the bremsstrahlung production target and the collimation system is given in Fig. 1.

Behind the flattening filter a thin segmented ionization chamber is mounted. The various segments of the chamber are used to control the position and flatness of the beam. In addition, because of the strong sensitivity of the photon angular distribution on the electron energy, the ratio between outer and inner segments of the ionization chamber is used to control the energy of the primary electron beam.

Between ionization chamber and the diaphragm system a so-called wedge filter may be used. This wedge leads to a well-defined asymmetric dose profile.

For the shaping of the photon beam according to the requirements of patient treatment a system of diaphragms in  $X$  and  $Y$  direction allows to define rectangular fields with a maximum size of  $40 \times 40 \text{ cm}^2$  at the nominal distance SSD = 100 cm. Additionally, a so-called multi-leaf collimator (MLC) allows to define irregular field shapes according to the clinical requirements. Together with the so-called wedge filter the diaphragm system requires about 35 cm space below the ionization chamber.

The ionization chamber is an essential part of the cLINAC and its beam control system. This restricts the positioning of the target samples for photoactivation

experiments to distances larger than about 20 cm from the almost point-like photon source. The diameter of the primary electron beam is typically less than 2 mm. For this closest position some parts of the cLINAC have to be removed; otherwise such a close target position is not accessible. Without any modification of the cLINAC, the closest target position is located at SSD  $\approx 55$  cm from the point-like photon source.

A typical cLINAC is able to provide electron beams at a number of fixed energies. The cLINAC under study is configured to provide primary electrons at  $E = 6$  MeV (X6) and 10 MeV (X10). A variation of the pre-defined fixed energies is possible by readjusting the operational parameters of the cLINAC. Because of the fully digital operation of the cLINAC under investigation, the pre-defined clinical beams can be restored within seconds by a software reload of the original parameters.

The clinical energy definition of a photon beam is given by the so-called beam quality factor which is derived from the measured depth dose curve in a water phantom. The standard definition of the beam quality factor  $Q$  uses a set-up with SSD = 100 cm from the practically point-like photon source to the surface of the water phantom and a field size of  $10 \times 10$  cm<sup>2</sup>. The beam quality factor is then defined by the ratio of doses  $D_{20}$  and  $D_{10}$  measured at a depth of 20 cm and 10 cm:

$$Q = D_{20}/D_{10} \tag{1}$$

Two typical depth-dose curves are shown in Fig. 2 for the available energies X6 and X10; the corresponding beam quality factors are  $Q = 0.685$  for X6 and  $Q = 0.732$  for X10. It has been shown that the stability of cLINACs is excellent. For the cLINAC under study we find very minor variations of  $Q$  of less than 1 % during typical irradiations with durations of a few minutes [25] and a long-time stability within  $\pm 1$  %.

By readjustment of the X10 beam parameters we have increased and decreased the electron energy. Two further depth dose profiles were measured where the changes in electron energy translate to slightly increased and reduced beam quality factors:  $Q_{>} = 0.738$  and  $Q_{<} = 0.727$ . These changes in  $Q$  correspond to a variation of the endpoint energy of about 500 keV. The depth dose profiles with increased  $Q_{>}$  and decreased  $Q_{<}$  are shown in Fig. 2 by dash-dotted lines. After restoring the original parameters of the X10 beam, a further depth dose curve was measured. This second curve with the original X10 parameters typically deviates by less than 0.1 % from the first X10 depth dose curve, and the beam quality factor of the second curve is  $Q = 0.732$  which is identical to the first measurement.

Under clinical conditions the cLINAC is able to provide a dose of slightly

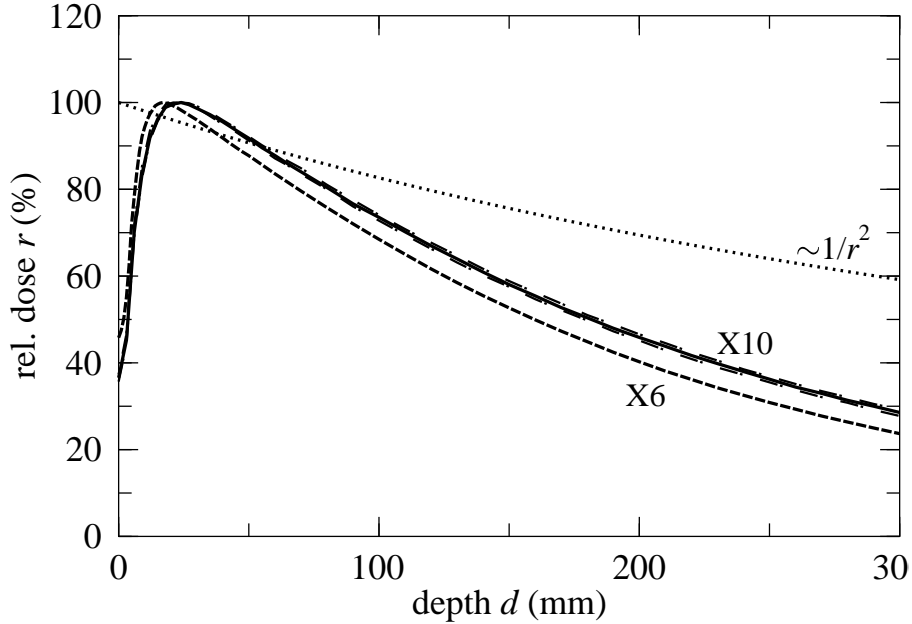


Fig. 2. Measured depth dose curves for two photon energies X6 (dashed line) and X10 (full line) corresponding to beam quality factors  $Q = 0.685$  and  $Q = 0.732$ . The dash-dotted lines show depth dose profiles for X10 with slightly increased  $Q_{>} = 0.738$  and reduced  $Q_{<} = 0.727$ ; these profiles have been measured using the predefined X10 beam with slightly modified parameters. For comparison the depth dependence for absorption-free radiation (proportional  $1/r^2$ ) is also shown (dotted line).

above 5 Gy per minute in the dose maximum of the depth dose curve in a water depth of about 1 – 2 cm. It is well-known that the average photon energy of bremsstrahlung from a cLINAC is about or slightly less than one third of the nominal endpoint energy [26]; i.e., for the X10 radiation in the present experiment one finds an average photon energy of about  $\bar{E} \approx 3$  MeV. A simple estimate of the photon intensity can be obtained as follows. From the depth dose curve in Fig. 2 (which includes the obvious  $1/r^2$  dependence) and its comparison to the  $1/r^2$  dependence it is possible to calculate that about 2.5% of the incoming photons are absorbed in a layer of 1 cm water. Thus, for delivery of 1 Gy in a  $10 \times 10$  cm<sup>2</sup> layer with 1 cm thickness a deposited energy of 0.1 J is required which corresponds to a primary energy of the photon beam of  $0.1 \text{ J}/0.025 = 4 \text{ J}$ . Together with the average photon energy of 3 MeV =  $4.8 \times 10^{-13}$  J one finds that  $8.3 \times 10^{12}$  incoming photons are required for the dose of 1 Gy in this layer with a volume of  $V = 100 \text{ cm}^3$ . This corresponds to  $8.3 \times 10^{10}$  photons per cm<sup>2</sup> or a photon intensity of about  $7 \times 10^9/(\text{cm}^2 \text{ s})$  for the delivery of 5 Gy in one minute. The spectral intensity is of the order of  $2 \times 10^6/(\text{keV cm}^2 \text{ s})$  assuming that the main intensity of a real bremsstrahlung spectrum is located between 1 and 5 MeV. The spectral intensity of more than  $10^6/(\text{keV cm}^2 \text{ s})$  is more than one order of magnitude higher than  $10^4 - 10^5/(\text{keV cm}^2 \text{ s})$  as e.g. stated in [27] for the S-DALINAC.

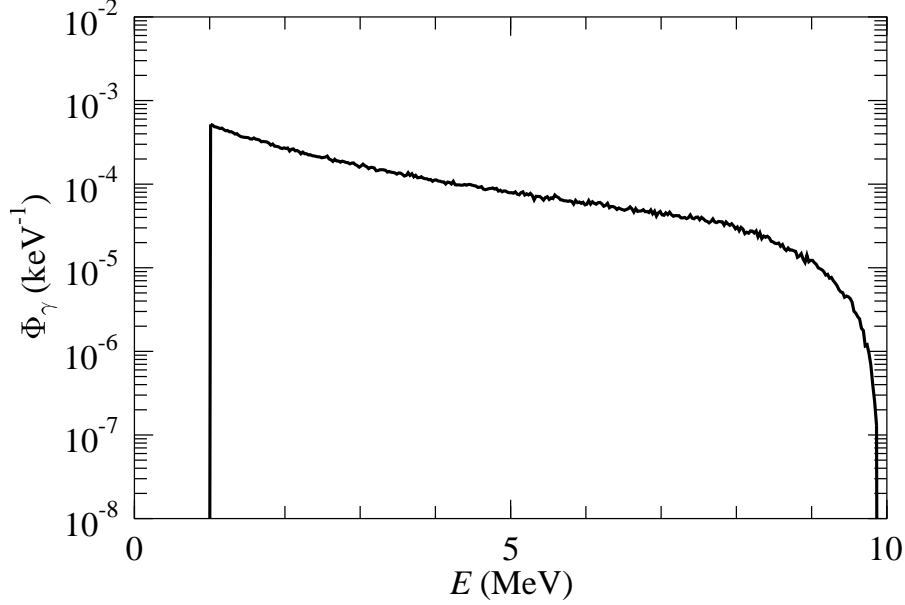


Fig. 3. Normalized energy distribution  $\Phi_\gamma(E)$  for thick-target bremsstrahlung with an endpoint energy  $E_0 = 9.9$  MeV from a GEANT simulation (calculation taken from [18]).

A typical energy distribution of bremsstrahlung is shown in Fig. 3. The energy distribution has been calculated for an electron energy of  $E_0 = 9.9$  MeV and a thick copper target [18] using the simulation code GEANT [28]. A lower cutoff of  $E = 1$  MeV was used in the simulation calculation to reduce the required time for the computation. The absorption of photons in the electron target and the flattening filter leads to a less sharp cutoff at similar energies in a realistic cLINAC [26]. The shown energy distribution  $\Phi_\gamma(E)$  is normalized to unity:

$$\int_0^{E_0} \Phi_\gamma(E) dE = 1 \quad (2)$$

The average energy

$$\bar{E} = \int_0^{E_0} E \Phi_\gamma(E) dE \quad (3)$$

for the shown spectrum in Fig. 3 is close to 3 MeV.

There is no perfect agreement between the calculated set-up in [18] and the cLINAC of the present work. However, it has been shown in [29] that the spectral shape of the energy distribution of bremsstrahlung depends only weakly on the details of the set-up. A very similar shape to Fig. 3 was obtained from

a simulation of a cLINAC in [26], and it has been shown that the calculated spectral shape of bremsstrahlung of cLINACs is close to measured energy spectra [26,30,31,32,33,34,35]. In particular, the spectral shape of a cLINAC close to the endpoint energy has been analyzed in [36,37], and a parametrization is given that corrects the simple Schiff formula for thin-target bremsstrahlung [38] to the spectral shape of a cLINAC [36].

Furthermore, a small variation in the energy of the primary electron beam can be taken into account in a simple way by a corresponding scaling the energy axis in Fig. 3 [29]. Such a scaling has been applied in the data analysis in Sect. 4.

### 3 Experimental Set-up

Two gold samples were irradiated for the present experiment. A thin foil with a thickness of  $3.7 \text{ mg/cm}^2$ , a size of  $40 \times 40 \text{ mm}^2$ , and a total weight of  $59.2 \text{ mg}$  was mounted at the target position without cLINAC modification at SSD  $\approx 55 \text{ cm}$  (see Fig. 1). A second target consisted of a larger amount ( $\approx 4 \text{ g}$ ) of irregularly shaped 333-gold (33.3% mass fraction of gold, other constituents are silver and copper in almost identical mass fractions). The second target was mounted at a slightly larger distance. The absolute photon intensity was determined from the activity of the thin gold foil whereas the decay spectrum and the half-life of the decaying activity were measured using the larger target with its higher count rates.

The irradiation time is software-restricted to a maximum of about 300 Gy corresponding to an irradiation time of about 55 minutes. This maximum irradiation time was used to activate the two gold targets by the  $^{197}\text{Au}(\gamma, n)^{196}\text{Au}$  reaction using the X10 photon beam. It is possible to extend the irradiation to longer times by a manual restart of the beam. However, as can be seen in the following, one hour irradiation time turned out to be sufficient for a measurable activation yield.

After irradiation the activity of the target samples was measured with a well-shielded standard NaI(Tl) detector. The  $\gamma$ -ray spectrum is shown in Fig. 4. Although the energy resolution of the NaI detector is not sufficient to resolve the two main decay lines at  $E_\gamma = 356 \text{ keV}$  and  $333 \text{ keV}$ , the signal-to-background ratio is very good because the integrated background in the shown energy range of the spectrum is below one count per second. The properties of the NaI detector are sufficient for the determination of the photon intensity in the present experiment. It is obvious that the NaI detector has to be replaced by a high-resolution detector for detailed photoactivation studies, particularly for target nuclei with low abundances or produced nuclei with long half-lives or



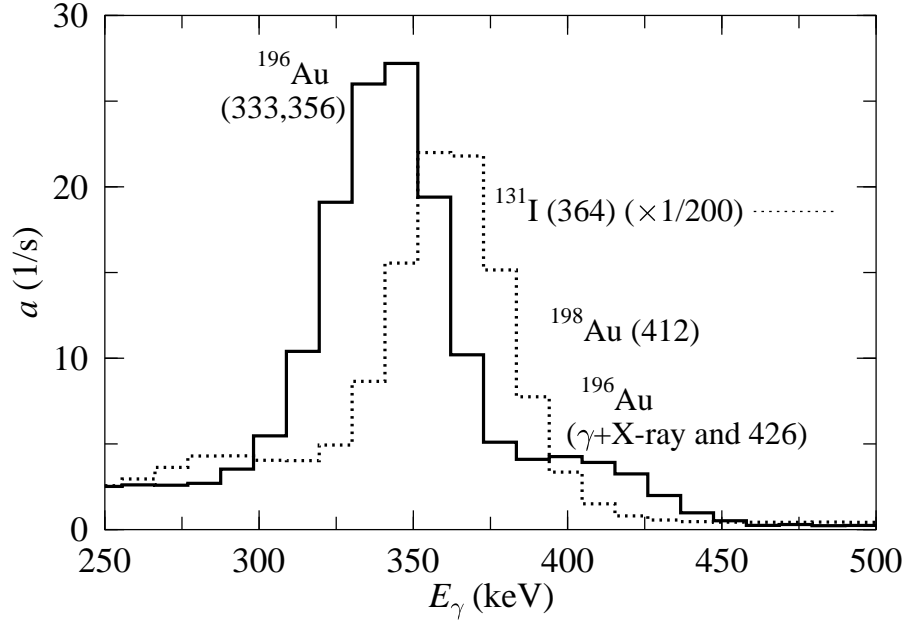


Fig. 4.  $\gamma$ -ray spectrum of the decay of  $^{196}\text{Au}$ , measured with a NaI detector. The energy resolution of the NaI detector is not sufficient to resolve the two main lines at 333 keV and 356 keV. Slightly above 400 keV a further peak can be seen which is composed of sum lines of X-rays and 333 keV or 356 keV, the weak decay line at 426 keV, and a decay line of  $^{198}\text{Au}$  which was produced by neutron capture in the  $^{197}\text{Au}(n,\gamma)^{198}\text{Au}$  reaction. Additionally, the calibration spectrum from  $^{131}\text{I}$  is shown with a dotted line.

weak  $\gamma$ -decay branches.

The absolute calibration for the NaI detector was performed with a calibrated source of  $^{131}\text{I}$ . The main  $\gamma$ -line from the decay of  $^{131}\text{I}$  at  $E = 364$  keV almost coincides with the  $\gamma$ -ray energies from the decay of  $^{196}\text{Au}$  at  $E = 356$  keV (branching per decay  $87.0 \pm 0.8\%$ ) and 333 keV ( $22.8 \pm 0.6\%$ ); note that the sum of the branchings exceeds 100% because of cascade transitions. For simplicity, a broad integration range of the spectrum from about 250 keV and 500 keV has been used in the data analysis. This window covers the main decay lines of  $^{196}\text{Au}$  and  $^{131}\text{I}$ . As pointed out above, the background in this broad energy window is below one count per second which has to be compared to the count rate of above 100 counts per second for the larger gold sample and more than 10 000 counts per second for the  $^{131}\text{I}$  calibration source where the deadtime of the NaI detector and its electronics is still below 5%.

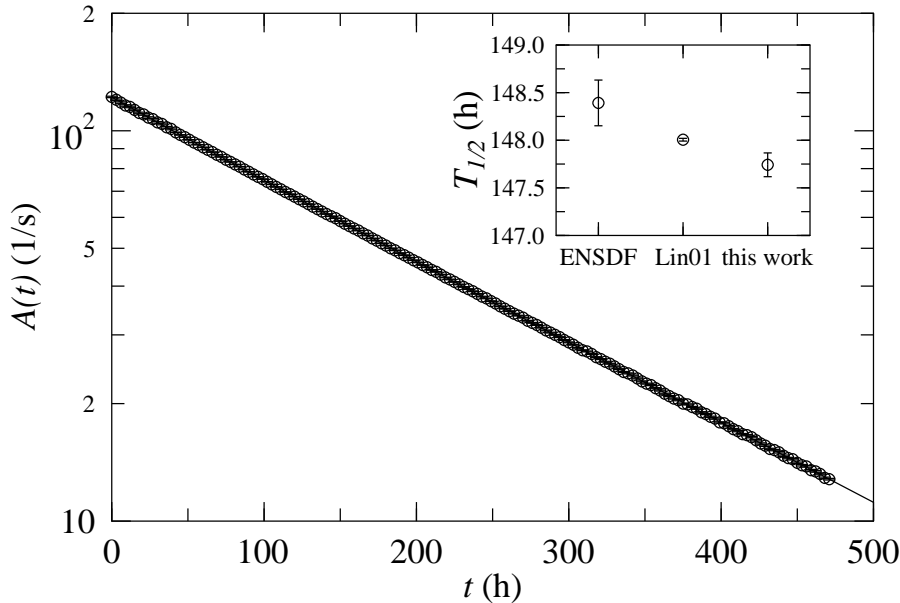


Fig. 5. Decay curve of the activity of  $^{196}\text{Au}$  measured over more than three half-lives. The inset compares our new result to the adopted value from the ENSDF data base [39,40] and the recently measured precise result of [41].

#### 4 Data analysis

In a first part of the data analysis the activity of the gold sample has been measured for more than three half-lives. The result is shown in Fig. 5. The obtained half-life of  $^{196}\text{Au}$  is  $T_{1/2} = 147.75 \pm 0.13$  h which is in rough agreement with the adopted value of  $148.39 \pm 0.24$  h [39,40] and overlaps within  $2\sigma$  with the recently measured precise number of  $148.006 \pm 0.015$  h [41]. It is interesting to note that a small component ( $< 5\%$ ) with a shorter half-life around 3 days is required for an excellent fit ( $\chi_{\text{red}}^2 \approx 1$ ) of the decay curve; this component comes probably from the decay of  $^{198}\text{Au}$  which can be produced by the  $^{197}\text{Au}(n,\gamma)^{198}\text{Au}$  reaction. A very weak decay line of  $^{198}\text{Au}$  was also observed in the  $\gamma$ -ray spectrum of [18]. The neutrons may have been produced in the target sample itself by the  $^{197}\text{Au}(\gamma,n)^{196}\text{Au}$  reaction and/or in the tungsten diaphragms of the cLINAC by the  $^{183,186}\text{W}(\gamma,n)^{182,185}\text{W}$  reactions.

The calculation of the photon intensity was performed as follows. The activity of the thin gold foil was measured after the irradiation to be 3.71 counts per second. The measured activity was converted to the number of produced  $^{196}\text{Au}$  nuclei taking into account the decay constant of  $^{196}\text{Au}$ , the  $\gamma$ -ray branching in the decay of  $^{196}\text{Au}$  and  $^{131}\text{I}$  which was used for the detector calibration, and the detector efficiency. The total number of  $^{197}\text{Au}(\gamma,n)^{196}\text{Au}$  reactions and produced  $^{196}\text{Au}$  nuclei was  $(2.38 \pm 0.25) \times 10^7$  where the uncertainty is dominated by the absolute calibration of the NaI detector.

The cross section of the  $^{197}\text{Au}(\gamma, n)^{196}\text{Au}$  reaction is well-known from the threshold at 8.071 MeV up to the giant dipole resonance. We use the parametrization of [18] which is based on the bremsstrahlung and photoactivation experiment of [18], one recent data point using LCS photons and direct neutron detection [14], and positron-in-flight annihilation experiment by [23]. The uncertainty of the  $^{197}\text{Au}(\gamma, n)^{196}\text{Au}$  reaction cross section is smaller than 5 % over the whole energy range of the present experiment.

The cross section, photon intensity, and number of reactions are related by the yield integral

$$N_R = k N_T \times \int_{S_n}^{E_0} \sigma(E) \Phi_\gamma(E, E_0) dE \quad (4)$$

with the number of reactions  $N_R$ , number of target atoms in the sample  $N_T$ , normalized bremsstrahlung spectrum  $\Phi_\gamma(E, E_0)$  at endpoint energy  $E_0$ , cross section  $\sigma(E)$ , and a scaling factor  $k$  for the normalized bremsstrahlung spectrum. The integral in Eq. (4) is limited by the neutron separation energy  $S_n$  and the endpoint energy  $E_0$ . The number of photons  $n_\gamma(E, E_0)$  (per keV and  $\text{cm}^{-2}$ ) for this irradiation is finally obtained by

$$n_\gamma(E, E_0) = k \times \Phi_\gamma(E, E_0) \quad (5)$$

The scaling factor  $k$  has been adjusted to reproduce the experimental yield. The result is shown in Fig. 6 for the distribution  $\Phi_\gamma(E, E_0 = 10 \text{ MeV})$  at SSD  $\approx 55 \text{ cm}$  (see also Fig. 3). The beam quality factor of  $Q = 0.732$  which was measured in the depth dose curve (see Fig. 2) indicates that the endpoint energy must be close to  $E_0 = 10 \text{ MeV}$ .

For experiments slightly above the  $(\gamma, n)$  threshold the results depend sensitively on the endpoint energy  $E_0$  in the experiment. Therefore, the above procedure for the determination of the scaling factor  $k$  and the number of photons  $n_\gamma(E, E_0)$  has been repeated using four normalized bremsstrahlung spectra  $\Phi(E, E_0)$  with different endpoint energies  $E_0 = 9, 10, 11, \text{ and } 12 \text{ MeV}$  which were obtained from the basic  $\Phi_\gamma(E, E_0 = 9.9 \text{ MeV})$  at the endpoint energy  $E_0 = 9.9 \text{ MeV}$  by a simple scaling of the energy axis (see Fig. 3). The results are also shown in Fig. 6 (dotted lines). It is obvious that a lower (higher) number of photons at higher (lower) endpoint energies  $E_0$  is required to fit the experimental photoactivation yield.

As a further check we used also a simplistic linear spectral shape between the energies of 8 and 10 MeV. The derived photon intensity from this simplistic spectral shape agrees at energies around 9 MeV within less than 10 % with the

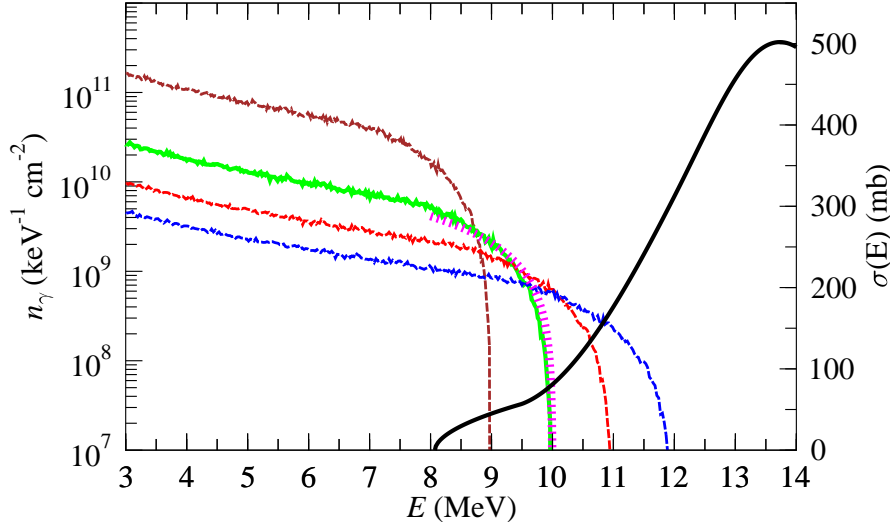


Fig. 6. Number of photons  $n_\gamma(E, E_0)$  at SSD  $\approx 55$  cm determined from the photoactivation yield in the  $^{197}\text{Au}(\gamma, n)^{196}\text{Au}$  reaction. The thick lines show the cross section of the  $^{197}\text{Au}(\gamma, n)^{196}\text{Au}$  reaction in the parametrization of [18] (right scale) and the photon intensity  $n_\gamma(E, E_0)$  for an endpoint energy of  $E_0 = 10$  MeV (left scale). Additionally, the dashed lines show the results for lower ( $E_0 = 9$  MeV) and higher ( $E_0 = 11$  and  $12$  MeV) endpoint energies for comparison. The hatched line represents a simplistic linear spectral shape between 8 and 10 MeV.

result using the spectral shape from the GEANT simulation with endpoint energy  $E_0 = 10$  MeV.

Using the realistic bremsstrahlung spectrum at  $E_0 = 10$  MeV, we find a number of photons of about  $n_\gamma \approx 2 \times 10^9 / (\text{keV cm}^2)$  at energies around 9 MeV for SSD  $\approx 55$  cm. These photons were irradiated within less than one hour. This corresponds to a photon intensity of about  $6 \times 10^5 / (\text{keV cm}^2 \text{ s})$  at  $E = 9$  MeV and SSD  $\approx 55$  cm. Because of the spectral shape of the bremsstrahlung spectrum, the number of photons at lower energies is much higher. E.g., around  $E = 3$  MeV we find  $n_\gamma \approx 3 \times 10^{10} / (\text{keV cm}^2)$  at SSD  $\approx 55$  cm which corresponds to an intensity of slightly below  $10^7 / (\text{keV cm}^2 \text{ s})$  at this SSD.

In Sect. 2 a rough estimate of the photon intensity of  $2 \times 10^6 / (\text{keV cm}^2 \text{ s})$  around 3 MeV was given for the distance of 100 cm between point-like photon source and water phantom (SSD = 100 cm). Consequently, for the smaller SSD of  $\approx 55$  cm of the photoactivation experiment one expects about a factor of four higher photon intensity, i.e.  $8 \times 10^6 / (\text{keV cm}^2 \text{ s})$ . This rough estimate from the dose absorption in a water tank is in excellent agreement with the number of slightly below  $10^7 / (\text{keV cm}^2 \text{ s})$  which was derived in the previous paragraph using the bremsstrahlung spectrum with  $E_0 = 10$  MeV. If one uses instead the bremsstrahlung spectrum at  $E_0 = 9$  MeV (11 MeV), one finds a photon intensity which is a factor of about five higher (three lower). This finding demonstrates the sensitivity of photoactivation yields at endpoint energies slightly

above the  $(\gamma, n)$  reaction threshold and confirms that the bremsstrahlung spectrum of the cLINAC has an endpoint energy close to  $E_0 = 10$  MeV.

Further study of the bremsstrahlung spectrum of the cLINAC is required to reduce the uncertainties of the above data analysis which are of the order about 25 % for the derived number of photons. For future experiments it might be helpful to establish a standard for the normalization of experiments which consists of several nuclei with different thresholds for the  $(\gamma, n)$  reaction. This can be done by measurements with quasi-monochromatic photons. At present precise data down to the threshold of the  $(\gamma, n)$  reaction are available e.g. for  $^{197}\text{Au}$  with  $S_n = 8071$  keV [18,14],  $^{187}\text{Re}$  with  $S_n = 7363$  keV [15,20,42], and  $^{186}\text{W}$  with  $S_n = 7194$  keV [43,15,19].

## 5 Discussion

The number of photons  $n_\gamma(E, E_0)$  – as shown in Fig. 6 for the SSD  $\approx 55$  cm – is sufficient to obtain a reasonable yield in  $(\gamma, n)$  experiments with measuring times of the order of one hour. Such experiments can be done easily at a cLINAC without major efforts for preparing the experiment. Reducing the SSD by almost a factor of three from 55 cm to about 20 cm at the close target position (see Fig. 1) leads to an increased photon intensity by almost one order of magnitude compared to the SSD of this experiment. However, this reduction of the SSD requires some preparation time and mechanical modifications which cannot be done easily at a cLINAC in daily clinical use.

A variation of the electron beam energy requires modification and optimization of the beam parameters which can be controlled by simultaneous measurements of depth dose profiles. Note that the beam quality factor of the depth dose profile is an excellent measure for the electron beam energy (see also Fig. 2). Although such modifications of the electron beam are possible in principle, the required effort and patient safety considerations will hamper larger series of photonuclear experiments at any cLINAC in routine clinical use because it must be absolutely sure that any modification of beam parameters for an experiment is removed before clinical use of the cLINAC. However, because the required beam time for photonuclear experiments is quite small, it seems nevertheless possible to perform larger series of photonuclear experiments e.g. during the set-up of a new cLINAC at the test facility of the manufacturer or at a newly installed cLINAC before clinical use.

Finally, radiation safety issues have to be considered before any larger experimental programs. Typically, the radiation protection of a cLINAC is calculated for a total dose of 1000 Gy per week (delivered at SSD = 100 cm) which is by far sufficient to treat about 50 patients per day with doses of 2 Gy. In clinical

use, most of the time is required for patient positioning, and the real irradiation time is quite short (typically far less than one minute per patient). The single irradiation of this experiment took about one hour and required a total dose of about 300 Gy. Such an irradiation corresponds to about one third of maximum dose per week, and obviously it cannot be performed several times a week.

However, the radiation safety problem may be solved or at least dramatically reduced. In clinical operation, the cLINAC is rotated around the patient. Radiation protection is designed so that 1000 Gy per week can safely be irradiated in any direction. Often one can find directions with much lower radiation exposure to the surrounding area. E.g., for the cLINAC under study the radiation exposure to the operators varies by about a factor 5 depending on the irradiation angle. It might be discussed with the regulatory authority to extend the radiation time by this factor of 5 at a well-defined radiation direction with low exposure to the operators. Additionally, the access to areas with high exposures may be prohibited or restricted in time.

## 6 Comparison to other electron accelerators and photon sources

The photon intensity which can be obtained without any modifications at SSD  $\approx 55$  cm is about one order of magnitude higher than the available intensity at the regular irradiation position at the S-DALINAC accelerator in Darmstadt [27]. Here simultaneous photon scattering [44] can be measured to reduce the uncertainties of the spectral shape of the photon spectrum. At a second irradiation position close to the photon source at S-DALINAC one finds a photon intensity which is a factor of 300 higher than at the standard irradiation position. This higher intensity is comparable to the increased intensity at a smaller SSD of the cLINAC of the present investigation.

The ELBE accelerator of Forschungszentrum Dresden is able to provide huge electron beam currents. However, at the standard irradiation position for nuclear resonance fluorescence experiments a thin radiator target is used leading to photon intensities of the order of  $5 \times 10^4 / (\text{keV s})$  at  $E = 7$  MeV for bremsstrahlung with  $E_0 = 10$  MeV [45]. A much higher photon intensity can be obtained at the beam dump of the high-current electron beam. A photon flux of “up to  $10^{10} \text{ cm}^{-2} \text{ s}^{-1} \text{ MeV}^{-1}$ ” is stated in [46] but the corresponding photon energy is not given in [46]. The determination of the energy spectrum of the bremsstrahlung and the absolute normalization of the bremsstrahlung are more complicated compared to the standard irradiation position. Nevertheless, a few remarkable experiments have been performed at ELBE. In particular, first experimental data for  $(\gamma, \alpha)$  reactions have been obtained [21].

There are a number of commercially available electron accelerators which may be equipped with a massive target for bremsstrahlung production. Electrostatic accelerators like dynamitrons and van-de-Graaf or pelletron accelerators provide high electron currents; however, the available energy is often limited. In particular, this is the case for single-ended electron accelerators. E.g. the S-Series pelletron from National Electrostatics Corporation (NEC) (“S” for single-ended) is limited to electron energies below 5 MeV [47]. The same limit of 5 MeV holds for the Radiation Dynamics (RDI) dynamitron [48]. Because of the limited electron energy photoactivation is practically restricted to isomers [3,4].

A high-power, high-energy electron accelerator, the so-called rhodotron accelerator (TT series), is available from Ion Beam Applications (IBA) [49] with energies of 10 MeV and beam power up to almost 200 kW. However, the only commercially available rhodotron with variable energy is limited to 7.5 MeV which is again too low for photoactivation experiments. Some development is needed for the 10 MeV rhodotron as an excellent energy-variable photon source. An energy-variable electron beam has to be implemented which is a complicated task, in particular for continuously varying electron energies.

Any comparison with quasi-monochromatic photon sources as e.g. AIST [50] at Tsukuba or HI $\gamma$ S [51] at Duke University, Durham, is difficult because the spectral intensity of quasi-monochromatic photon sources is very high (or infinity for an ideal monochromatic photon source). However, the absolute number of photons is typically lower compared to bremsstrahlung facilities. It depends on the requirements of the respective experiment whether a quasi-monochromatic photon source or a bremsstrahlung photon source is to be preferred.

Recently, a new high-intensity non-monochromatic photon source was suggested using synchrotron radiation from a 10 T superconducting wiggler at a many-GeV electron storage ring at SPring-8 [22]. A first proposal has been accepted, and hopefully this first part of the MeV photon source will become operational within the next years. The properties of this outstanding photon source cannot be reached by a cLINAC but it can be expected that the beamtime at such a huge facility will be very limited.

## 7 Conclusions

A photon intensity of about  $6 \times 10^5 / (\text{keV cm}^2 \text{ s})$  at  $E = 9 \text{ MeV}$  can be achieved at the cLINAC under investigation without any modification to the clinical setup. The photon intensity may be increased by almost one order of magnitude by minor modifications. This intensity is at least comparable to photon sources

which have been used in recent photonuclear experiments.

Furthermore, the excellent stability and reproducibility of the beam of a cLINAC are good prerequisites for such experiments. The required beam times are short and can be done during the night when most cLINACs are not in operation.

In summary, a cLINAC is an excellent photon source for photonuclear experiments. Besides the radiation safety problem, there is not any physical argument that stands against photonuclear research at a cLINAC.

## Acknowledgments

We thank Th. Aller for his assistance and patience during the measurements of the  $\gamma$ -ray spectra, the group *Physik in der Medizin* from Gymnasium St. Michael (M. Amend, A. Angerer, J. Bahmüller, J. Förstel, B. Franz, N. Pohl, J. Scheu, A. Sebek, L. Zipperer) for their help in the experiment, and Th. Preisendanz for the support of this project.

## References

- [1] Proc. *11th International Conference on Modern Trends in Activation Analysis (MTAA-11)*, Surrey, Guildford, J. Radioanal. Nucl. Chem. **271** (2007).
- [2] K. Masumoto and Ch. Segebade, in *Encyclopedia of Analytical Chemistry*, ed. R. A. Meyers, Wiley Interscience (2000), doi 10.1002/9780470027318.a6211.
- [3] K. X. Nghiem and L. Lakosi, J. Radioanal. Nucl. Chem. **230**, 143 (1998).
- [4] D. Belic *et al.*, Nucl. Inst. Meth. Phys. Res. A **463**, 26 (2001).
- [5] T. Webb, W. Beezhold, L. DeVeaux, F. Harmon, J. Petrisko, R. Spaulding, R. Assink, Proc. *Particle Accelerator Conference PAC 2005*, p. 2363 (2005).
- [6] S. E. Woosley and W. M. Howard, *Astroph. J. Suppl.* **36**, 285 (1978).
- [7] D. L. Lambert, *Astron. Astrophys. Rev.* **3**, 201 (1992).
- [8] T. Rauscher, A. Heger, R. D. Hoffman, and S. E. Woosley, *Astroph. J.* **576**, 323 (2002).
- [9] M. Arnould and S. Goriely, *Phys. Rep.* **384**, 1 (2003).
- [10] T. Hayakawa, N. Iwamoto, T. Shizuma, T. Kajino, H. Umeda, and K. Nomoto, *Phys. Rev. Lett.* **93**, 161102 (2004).



- [11] H. Utsunomiya, P. Mohr, A. Zilges, M. Rayet, Nucl. Phys. **A777**, 459 (2006).
- [12] P. Mohr, K. Vogt, M. Babilon, J. Enders, T. Hartmann, C. Hutter, T. Rauscher, S. Volz, A. Zilges, Phys. Lett. B **488**, 127 (2000).
- [13] P. Mohr, Zs. Fülöp, H. Utsunomiya, Europ. Phys. J. A **32**, 357 (2007).
- [14] H. Utsunomiya, H. Akimune, S. Goko, M. Ohta, H. Ueda, T. Yamagata, K. Yamasaki, H. Ohgaki, H. Toyokawa, Y.-W. Lui, T. Hayakawa, T. Shizuma, E. Khan, and S. Goriely, Phys. Rev. C **67**, 015807 (2003).
- [15] T. Shizuma, H. Utsunomiya, P. Mohr, T. Hayakawa, S. Goko, A. Makinaga, H. Akimune, T. Yamagata, M. Ohta, H. Ohgaki, Y.-W. Lui, H. Toyokawa, A. Uritani, and S. Goriely, Phys. Rev. C **72**, 025808 (2005).
- [16] S. Goko, H. Utsunomiya, S. Goriely, A. Makinaga, T. Kaihori, S. Hohara, H. Akimune, T. Yamagata, Y.-W. Lui, H. Toyokawa, A. J. Koning, and S. Hilaire, Phys. Rev. Lett. **96**, 192501 (2006).
- [17] H. Utsunomiya, A. Makinaga, S. Goko, T. Kaihori, H. Akimune, T. Yamagata, M. Ohta, H. Toyokawa, S. Müller, Y.-W. Lui, and S. Goriely, Phys. Rev. C **74**, 025806 (2006).
- [18] K. Vogt, P. Mohr, M. Babilon, W. Bayer, T. Hartmann, C. Hutter, T. Rauscher, K. Sonnabend, S. Volz, A. Zilges, Nucl. Phys. **A707**, 241 (2002).
- [19] K. Sonnabend, K. Vogt, D. Galaviz, S. Müller, and A. Zilges, Phys. Rev. C **70**, 035802 (2004).
- [20] S. Müller, A. Kretschmer, K. Sonnabend, A. Zilges, D. Galaviz, Phys. Rev. C **73**, 025804 (2006).
- [21] A. Wagner, R. Beyer, M. Erhard, F. Dönau, E. Grosse, A. Hartmann, A.R. Junghans, L. Käubler, K. Kosev, S. Mallion, C. Nair, N. Nankov, G. Rusev, K.D. Schilling, W. Schulze and R. Schwengner, J. Phys. G **31**, S1969 (2005).
- [22] H. Utsunomiya, S. Goko, K. Soutome, N. Kumagai, and H. Yonehara, Nucl. Inst. Meth. Phys. Res. A **538**, 225 (2005).
- [23] B. L. Berman, R. E. Pywell, S. S. Dietrich, M. N. Thompson, K. G. McNeill, J. W. Jury, Phys. Rev. C **36**, 1286 (1987).
- [24] Elekta Digital Accelerator, Technical Training Guide, 2003 (unpublished).
- [25] P. Mohr, S. Brieger, J. Stahl, G. Witucki, Strahlenth. Onkol. **183**, 327 (2007).
- [26] F. Verhaegen and J. Seuntjens, Phys. Med. Biol. **48**, R107 (2003).
- [27] P. Mohr, J. Enders, T. Hartmann, H. Kaiser, D. Schiesser, S. Schmitt, S. Volz, F. Wissel, A. Zilges, Nucl. Inst. Meth. Phys. Res. A **423**, 480 (1999).
- [28] Software package *GEANT Detector description and simulation tool*, <http://wwwinfo.cern.ch/asd/geant/>.

- [29] K. Vogt, P. Mohr, M. Babilon, J. Enders, T. Hartmann, C. Hutter, T. Rauscher, S. Volz, and A. Zilges, Phys. Rev. C **63**, 055802 (2001).
- [30] R. Mohan, C. Chui, and L. Lidofski, Med. Phys. **12**, 592 (1985).
- [31] A. B. Faddegon, C. K. Ross, D. W. O. Rogers, Med. Phys. **17**, 773 (1990).
- [32] A. B. Faddegon, C. K. Ross, D. W. O. Rogers, Med. Phys. **18**, 727 (1991).
- [33] A. B. Faddegon and D. W. O. Rogers, Nucl. Inst. Meth. Phys. Res. A **327**, 556 (1993).
- [34] D. Sheikh-Bagheri and D. W. O. Rogers, Med. Phys. **29**, 379 (2002).
- [35] D. Sheikh-Bagheri and D. W. O. Rogers, Med. Phys. **29**, 391 (2002).
- [36] M. Krmar, D. Nikolic, P. Krstonosic, S. Cora, P. Francescon, P. Chiovati, A. Rudic, Med. Phys. **29**, 932 (2002).
- [37] M. Krmar, K. Ganezer, G. Pantelic, P. Krstonosic, Nucl. Inst. Meth. Phys. Res. A **532**, 533 (2004).
- [38] L. I. Schiff, Phys. Rev. **83**, 252 (1951).
- [39] Web data base ENSDF <http://www.nndc.bnl.gov/ensdf/>, Brookhaven National Laboratory, Version April 5<sup>th</sup>, 2007.
- [40] H. Ikegami, K. Sugiyama, T. Yamazaki, M. Sakai, Nucl. Phys. **41**, 130 (1963).
- [41] K. Lindenberg, F. Neumann, D. Galaviz, T. Hartmann, P. Mohr, K. Vogt, S. Volz, A. Zilges, Phys. Rev. C **63**, 047307 (2001).
- [42] P. Mohr, S. Goriely, T. Shiyuma, T. Hazakawa, PoS(NIC-IX) 142 (2007).
- [43] P. Mohr, T. Shizuma, H. Ueda, S. Goko, A. Makinaga, K. Y. Hara, T. Hayakawa, Y.-W. Lui, H. Ohgaki, and H. Utsunomiya, Phys. Rev. C **69**, 032801(R) (2004).
- [44] U. Kneissl, H. H. Pitz, and A. Zilges, Prog. Part. Nucl. Phys. **37**, 349 (1996).
- [45] A. Wagner, <http://www.fzd.de/ELBE> (2006).
- [46] M. Erhard, A. R. Junghans, R. Beyer, E. Grosse, J. Klug, K. Kosev, C. Nair, N. Nankov, G. Rusev, K. D. Schilling, R. Schwengner, and A. Wagner, Europ. Phys. J. A **27**, s01, 135 (2006).
- [47] <http://www.pelletron.com/sseries.htm>.
- [48] <http://www.iba-worldwide.com/rdi/>.
- [49] <http://www.iba-worldwide.com/industrial/product-range/rhodotron/index.php>.
- [50] H. Ohgaki, S. Sugiyama, T. Yamazaki, T. Mikado, M. Chiwaki, K. Yamada, R. Suzuki, T. Noguchi, T. Tomimasu, IEEE Trans. Nucl. Sci. **38**, 386 (1991).
- [51] H. R. Weller and M. W. Ahmed, Mod. Phys. Lett. A **18**, 1569 (2003).